Journal of Catalysis **209,** 433–444 (2002)
doi:10.1006/jcat.2002.3629

Structure, Acidity, and Catalytic Activity of Mesoporous Acid Catalysts for the Gas-Phase Synthesis of MTBE from MeOH and Bu^{t}OH

Q.-H. Xia,*,[1] K. Hidajat,† and S. Kawi†

*Institute of Chemical Sciences, #02-08, Block 28, Ayer Rajah Crescent, Singapore 139959; and †Department of Chemical & Environmental Engineering, National University of Singapore, Singapore 119260

Received December 14, 2001; revised March 11, 2002; accepted April 3, 2002

The regular mesostructure of Si–MCM-41 with a uniform mesopore size is well maintained after 50 wt% HPW loading that was highly dispersed onto Si–MCM-41, without an HPW crystalline phase being detected by XRD. An HPW-supported mesoporous catalyst (HPW/MCM-41) shows excellent catalytic activity and on-stream stability for the gas-phase synthesis of MTBE at temperatures below 100°C. The surface acidity and hydrophobicity of the HPW/MCM-41 catalysts are enhanced stepwise by increasing the HPW loading. The ratio of Brønsted acidity to Lewis acidity on HPW/MCM-41 is adjustable by varying the amounts of HPW. The catalytic activity of various mesoporous catalysts showed the following order: Amberlyst-15 ≈ HPW (50%)/MCM-41 > H_2SO_4/MCM-41 > HAlMCM-41 > SO_4^{2-}/ZrO_2/MCM-41 > NaAlMCM-41 ≫ Si–MCM-41, corresponding to the importance of their surface acidity. The exception of SO_4^{2-}/ZrO_2/MCM-41 in this arrangement may be related to the complexity of sulfated-ZrO_2 superacid. The rapid deactivation of the H_2SO_4/MCM-41 catalyst is ascribed to the leaching of mobile H_2SO_4 molecules on Si–MCM-41 during the reaction. © 2002 Elsevier Science (USA)

Key Words: **HPW/MCM-41; heteropoly acid; HAlMCM-41; mesoporous solid acid; acidity; gas-phase synthesis of MTBE.**

INTRODUCTION

Due to its high octane number, MTBE (methyl-*tert*-butyl ether) is presently the most widely used additive for improving the quality of unleaded gasolines (1, 2). The decomposition of the ether is also of industrial interest, as it represents a route to producing pure isobutene (1). The worldwide production of MTBE has increased faster than most other commodity chemicals, with a total capacity of about 18.5×10^6 tons and an estimated increasing yearly demand of 15% (1, 3). However, MTBE is being scrutinized for potential damage to groundwater and atmosphere (4–7). In the near future, the use of MTBE will be reduced and could be replaced by ethanol, other oxygenates, or highly branched hydrocarbons, which are less harmful to the environment (8, 9).

MTBE is industrially synthesized from methanol and isobutene over a sulfonated ion-exchange resin such as Amberlyst-15 (10) or through reacting *tert*-butanol (Bu^{t}OH) with methanol (MeOH) over an acidic catalyst yielding the desired MTBE with water as a coproduct (11). Since the Amberlyst-15 catalyst used in this synthesis has severe drawbacks, such as being thermally and chemically unstable (12, 13), many acidic catalysts, such as traditional microporous zeolites, sulphated-ZrO_2 catalysts, and heteropoly acids (HPAs), have been developed to catalyze these reactions (1, 2, 14–16). Zeolites have been investigated as potential alternative catalysts for MTBE formation; however, most of the zeolites are less efficient catalysts than Amberlyst-15 (2, 12, 17–19), and only beta zeolite is nearly as active as the resin (20).

The use of relatively stable and strongly acidic heteropoly acids in acid-catalyzed reactions has attracted increasing attention for processes requiring higher acidity than that of the zeolites (21–24). In particular, the 12-tungstophosphoric acid $H_3PW_{12}O_{40}$ (HPW) is the most acidic of the Keggin series (25). This has led most researches to focus on HPW acid. However, for heteropoly acids to be effective as catalysts they should be supported on a carrier with a large surface area due to the extremely small surface area (<10 m^2/g) of these nonporous materials (22, 26). Even though silica, alumina, resin, active carbon, clays, and microporous zeolites are used as supports (27–30), their nonuniform pore size and relatively small surface area limit their potential for catalyzing bulky molecules because of diffusion problems. Owing to a very large surface area (typically ~1000 m^2/g) and a uniform large pore size (>15Å), the M41s materials (31) are excellent supports for preparing bifunctional catalysts (32–35) and for expanding the catalytic capability of traditional acidic materials for some applications (26, 36–38). This is because such mesoporous materials, which have relatively small diffusion hindrance, can aid the easy diffusion of bulky organic molecules in and out of their mesopores (38). The studies have also shown that SiAlMCM-41 possesses both Brønsted and Lewis acid sites and is catalytically active in some reactions (39–42). Several recent reports have been

[1] To whom correspondence should be addressed.

0021-9517/02 $35.00

published on HPW/MCM-41 systems that catalyze reactions such as the alkylation of isobutene by butene (26) and 4-*tert*-butylphenol by isobutene and styrene (36), and the conversion of 1,3,5-triisopropylbenzene (37). However, HPW/MCM-41 catalysts have not yet been used in the gas-phase synthesis of MTBE.

Very recently, the SO_4^{2-}/ZrO_2/MCM-41 catalyst was reported to show high activity and excellent on-stream stability for this reaction below 160°C (38). However, the catalytic activity of this catalyst was lower than that of the commercial Amberlyst-15 catalyst, which was attributed to its weak surface acidity. The research reported here focused mainly on the gas-phase synthesis of MTBE from MeOH and Bu^{t}OH over various mesoporous acidic catalysts and on the contribution of surface acidity to the activity of catalysts. HPW/MCM-41 was first applied to catalyze the gas-phase synthesis of MTBE from MeOH and Bu^{t}OH, and the effect of HPW loading on the structure, acidity, and activity of HPW/MCM-41 acidic catalysts was investigated in detail. The results show that the catalytic activity of HPW (30%)/MCM-41 and HPW (50%)/MCM-41 is comparable to that of commercial Amberlyst-15.

EXPERIMENTAL

Preparation of Mesoporous Acidic Catalysts

The support, fluorinated Si–MCM-41 with excellent hydrothermal stability, was synthesized in a fluoride medium (43, 44). The preparation of the acidic catalyst SO_4^{2-}/ZrO_2/MCM-41 with 41.0 wt% ZrO_2 (ICP analysis) and 9.10 wt% sulphate (TGA analysis) was described elsewhere (38). H_2SO_4/MCM-41 was prepared by dispersing 0.75 g of Si–MCM-41 (predried at 96°C overnight) in 50 ml of sulfuric acid solution (5 N) under vigorous stirring. After 1 h, the solution was filtered off, and the recovered solid was dried at 96°C overnight, followed by calcination at 300°C for 3 h in air. TGA analysis showed that the weight loss between 300 and 1000°C of the prepared H_2SO_4/MCM-41 was 5.45 wt%. A commercial sulfonated ion-exchange resin Amberlyst-15 (Merck), with an acidity of 4.7 meq/g dry, was used as a reference catalyst.

Na,Al-containing MCM-41 was synthesized according to the synthesis procedure reported elsewhere (44). The resulting material, NaAlMCM-41, was calcined at 580°C for 10 h and ion exchanged into HAlMCM-41. One gram of NaAlMCM-41 was mixed with 20 ml of a 15-wt% acetic acid solution, and an appropriate volume of it was placed into a beaker containing a fine powder of NaAlMCM-41 under continuous stirring. After 3 h, the solution was filtered off and the solid was washed four times with deionized water. This ion-exchange procedure was repeated three times. The recovered solid was dried at 96°C overnight and calcined at 300°C for 4 h in nitrogen, followed by 4 h in air at 550°C. Using ICP, the Si : Al molar ratios of NaAlMCM-41 and HAlMCM-41 were found to be 22 and 25, respectively.

HPW was supported by impregnation of fluorinated Si–MCM-41. One gram of predried Si–MCM-41 (at 300°C overnight) powder with a BET surface area of 1311 m^2/g and a pore size of 31.4 Å was dispersed under vigorous stirring into a solution of the desired amount of HPW crystals (Merck) in 12 ml of water. The pH value of the resulting solution was between 1 and 2, which is crucial, because Keggin HPAs are known to decompose into lacunary $PW_{11}O_{39}^{7-}$ (PW_{11}) species in aqueous solutions at pH above 2 (25). After evaporating the water at 70°C, the solid was dried in an oven at 96°C overnight and at 120°C for 2 h, followed by calcination at 300°C for 5 h in air. Three HPW (x%)/MCM-41 catalysts, where x% is the respective HPW content of 15, 30, and 50 wt%, were prepared according to the same procedure. Note that after calcination at 300°C in air, the pure HPW turned light brown; the calcined HPW, however, dissolved in water to give a colorless clear solution again.

Characterisation of Catalysts

The XRD patterns of powdered samples were recorded between 1.5 and 70° 2θ with a Shimadzu XRD-6000 diffractometer using Ni-filtered Cu $K\alpha$ radiation operating at 40 kV and 30 mA. Autosorb-1 was used to measure the N_2 adsorption–desorption isotherms of the samples. Prior to the measurements, the samples were degassed at 300°C overnight. The BET specific surface area was calculated using the BET equation in the range of relative pressures between $p/po = 0.05$ and 0.25. The BJH method was used to calculate the pore volume and the pore size distribution of the samples. The weight loss curves (TGA analysis) of the catalysts were recorded on a Shimadzu DTG-50 thermogravimetric analyzer at a heating rate of 20°C/min, from room temperature to 1000°C in an air flow of 50 ml/min.

The *in situ* FTIR spectra of the S=O vibrational band, hydroxyl groups, and pyridine chemisorption were recorded using a Shimadzu FTIR-8700 spectrophotometer with a resolution of 4 cm^{-1} and connected to a PFEIFFER vacuum system. Before scanning the IR spectra of the S=O vibration and hydroxyl groups, a self-supporting wafer (16 mg, with a pressure of 5 ton cm^{-2}) of the catalyst was evacuated at 300°C for 5 h in an *in situ* cell under a residual pressure of 10^{-6} mbar. The relative coverage of surface hydroxyl groups of the HPW/MCM-41 catalysts was evaluated by comparing the integrated area of the hydroxyl bands (3000–3750 cm^{-1}) to that of the Si–MCM-41 support. IR spectra of adsorbed pyridine were recorded to determine the presence of Brønsted and Lewis acid sites over the catalysts. A self-supporting wafer (16 mg) of the catalyst was heated at 300°C for 3 h under a residual pressure of 10^{-6} mbar before adsorbing an excess of pyridine at room temperature, followed by evacuation at 200°C for 30 min. Brønsted and Lewis acidities were quantified from the integrated areas

of the bands at 1540 and at 1445 cm^{-1}, respectively. The integrated areas of these two bands provide information only about the relative amount of pyridine, which interacts with Brønsted and Lewis sites; therefore the B, L, and B/L values must be regarded as relative indications.

The FTIR spectra of pure HPW and supported HPW/MCM-41 were recorded between 400 and 4000 cm^{-1} using KBr disks at ambient temperature. The resolution was 4 cm^{-1}. ICP elemental analysis was performed with a Perkin–Elmer Optima 3000DV Spectrometer. Calibration standards with different concentrations were prepared by diluting corresponding standard metal solutions.

Catalytic Tests

For the gas-phase synthesis of MTBE from MeOH and Bu^tOH in a continuous fixed-bed reactor, 0.20 g of the catalyst (40–60 mesh fraction) was predehydrated at 300°C for 2 h in a flow of helium before a mixture of MeOH and Bu^tOH, with a molar ratio of 10 : 1, was pumped by an ISCO syringe pump into the reactor (1/4 in. o.d.) and heated at the given temperatures. During the reaction, a 13-ml/min helium flow was used as the carrier and diluting gas, and the weight hourly space velocity (WHSV) was kept at 10 h^{-1}. Each reaction reached steady state in 30 min; the products were then analyzed on stream by a Shimadzu GC-17A gas chromatograph equipped with a FID and an OV-1 capillary column. The conversion (mole percent) of Bu^tOH to MTBE, i.e., the selective conversion of Bu^tOH to MTBE, was equal to the actual steady conversion of Bu^tOH (mole percent) into the products times the selectivity of MTBE (percent), regardless of excessive amounts of MeOH. The selectivity of MTBE below the optimal temperature is 100% for each reaction, thereafter decreasing gradually with increasing temperature.

RESULTS AND DISCUSSION

Effect of HPW Loading on HPW/MCM-41 Acidic Catalysts

Structure of HPW/MCM-41 Catalysts

For pure HPW, calcined and not calcined at 300°, about 15 intense diffraction peaks were clearly distributed between $2\theta = 5$ and 65° (Fig. 1). These diffraction peaks can be indexed to the typical Keggin structure of HPAs, showing that the calcination treatment does not destroy the crystalline structure of HPW. The XRD patterns of Si–MCM-41 and the three HPW/MCM-41 samples show four [100], [110], [200], and [210] diffraction peaks below 10° 2θ. This indicates that the long-range ordering of the hexagonal mesostructure of the Si–MCM-41 support is maintained, even after impregnation of 50 wt% HPW in acidic solution and then calcination at 300°C. However, the amount of HPW has a remarkable effect on the intensity of the

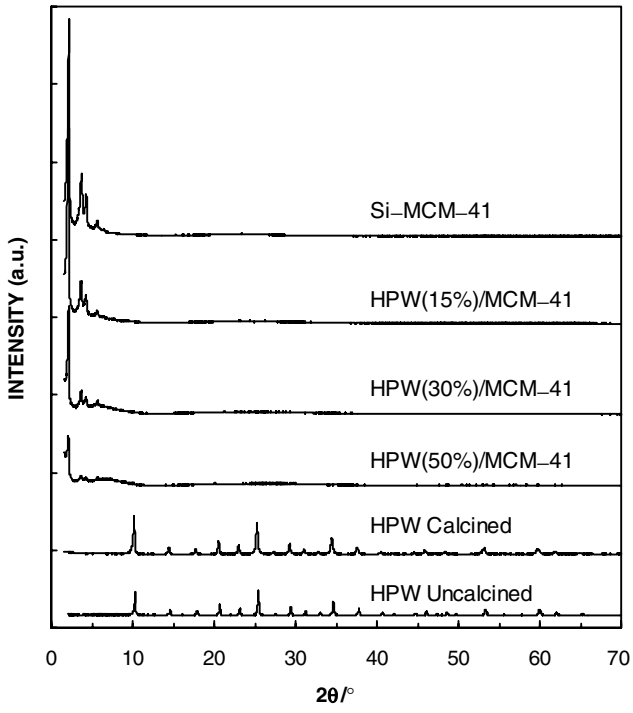

FIG. 1. The effect of HPW loading on the XRD patterns of HPW/MCM-41 samples and on the crystalline phase of HPW on HPW/MCM-41.

main [100] reflection peak of the Si–MCM-41 support, and the peak height is inversely proportional to the amount of loaded HPW. With increasing HPW loading, from 15 to 50 wt%, a featureless broad bump appears in the region $2\theta = 15$–40°; another bump gradually rises at $2\theta = 5$–10°, which can be ascribed to the formation of amorphous phases. No crystalline HPW diffraction is observed above 10° 2θ, indicating that most of the HPW was highly dispersed on the Si–MCM-41. This differs from the observations reported in the literature (37), where once loaded with HPW, the MCM-41 support lost its regular mesostructure, and the HPW loading over 23 wt% led to a total collapse of the MCM-41 structure and observable crystalline HPW XRD peaks. This improvement is attributed to the use of well-ordered MCM-41 in our study.

Table 1 shows that for the HPW/MCM-41 samples the BET surface area and the pore volume reduce rapidly with increasing HPW loading. The BET surface area and pore volume of Si–MCM-41 and all the HPW/MCM-41 samples decrease in the following order: Si–MCM-41 > HPW (15%)/MCM-41 > HPW (30%)/MCM-41 > HPW (50%)/MCM-41 ≫ pure HPW. Pure HPW is a nonporous crystalline material with a BET surface area smaller than 10 m^2/g; however, once loaded onto Si–MCM-41, the resulting HPW/MCM-41 porous materials have a BET surface area above 500 m^2/g, with a pore volume of more than 0.40 cm^3/g. With increasing HPW loading, from 15 to 50 wt%, the BET surface area and pore volume of the

TABLE 1

BET Data and Mesostructures of Various Mesoporous Samples

Sample	BET surface area (m^2/g)	Pore volume (cm^3/g)	Pore diameter (Å)	Mesopor. phase[a]	HPW phase[a]
Si–MCM-41	1311	1.03	31.4	MCM-41	
HPW (15%)/MCM-41	1128	0.98	30.0	MCM-41	Amorphous
HPW (30%)/MCM-41	632	0.53	29.7	MCM-41	Amorphous
HPW (50%)/MCM-41	499	0.40	29.5	MCM-41	Amorphous
Pure HPW	<10				Crystalline
H_2SO_4/MCM-41	1221	1.01	31.1	MCM-41	
NaAlMCM-41	1257	1.01	28.0	MCM-41	
HAlMCM-41	1122	0.99	26.7	MCM-41	
SO_4^{2-}/ZrO_2/MCM-41	688	0.58	29.1	MCM-41	
Amberlyst-15	50	0.05	—[b]	—[b]	

[a] The mesoporous phase and the HPW phase are detected by XRD.
[b] Not detectable.

three HPW/MCM-41 samples decreases to 1128, 632, and 499 m^2/g and to 0.98, 0.53, and 0.40 cm^3/g, respectively. However, the HPW/MCM-41 samples display a fairly uniform size distribution of the mesopores centered at about 29.5–30.0 Å. The pore sizes of the HPW/MCM-41 samples are 1.4–1.9 Å, smaller than that of Si–MCM-41. This shows that HPW has been dispersed onto the surface of the mesopores of Si–MCM-41. However, a very slow decrease in pore size with increasing HPW loading indicates that the abrupt decrease in the BET surface area and pore volume at higher loadings of HPW is due to the partial blockage of one-dimensional mesopores of Si–MCM-41 by small aggregates of HPW.

Figure 2 shows the N_2 adsorption–desorption isotherms of Si–MCM-41 and all the HPW/MCM-41 samples. The hysteresis loops of the HPW/MCM-41 samples were, for the most part, not detected by our method. A sharp mesoporous inflection was observed on the isotherms of these samples at a relative pressure between $p/po = 0.25$ and 0.40. With increasing HPW loading, the inflection became gradually shorter, corresponding to a reduction in the pore volume. As shown in Fig. 2, a notable compression of the pore sizes distribution with increasing HPW loading was revealed.

Figure 3 shows the IR spectrum (KBr pellets) of pure HPW with a Keggin structure with four strong bands, at 1082 (P–O), 988 (W=O), 891, and 800 (W–O–W) cm^{-1}, and one weak band at 525 cm^{-1} (W–O–P) (36). The framework bands of Si–MCM-41 at 1236, 1090, 965, 800, 564, and 465 cm^{-1} (43) easily overlap with those of HPW. For HPW (15%)/MCM-41, none of the HPW bands was observable except for a slight increase in the intensity of the 800 cm^{-1} band. For an HPW loading of 30 wt%, the bands at 988 and 891 cm^{-1} became visible. With 50% of HPW loading, the 1082-cm^{-1} band became sharper and the intensity of the two bands at 988 and 891 cm^{-1} increased. Furthermore, it was observed that the intensity of the 800-cm^{-1} band was almost proportional to the increase in the amount of HPW on MCM-41 due to the greater number of oscillators. The FTIR spectra of the Keggin structure of HPW/MCM-41 with different HPW loading clearly differ from those reported in the literature (36, 37). In those studies, the strongest framework band of Si–MCM-41 at 1090 cm^{-1} was not observed, possibly due to the loss of the crystalline organization of the support.

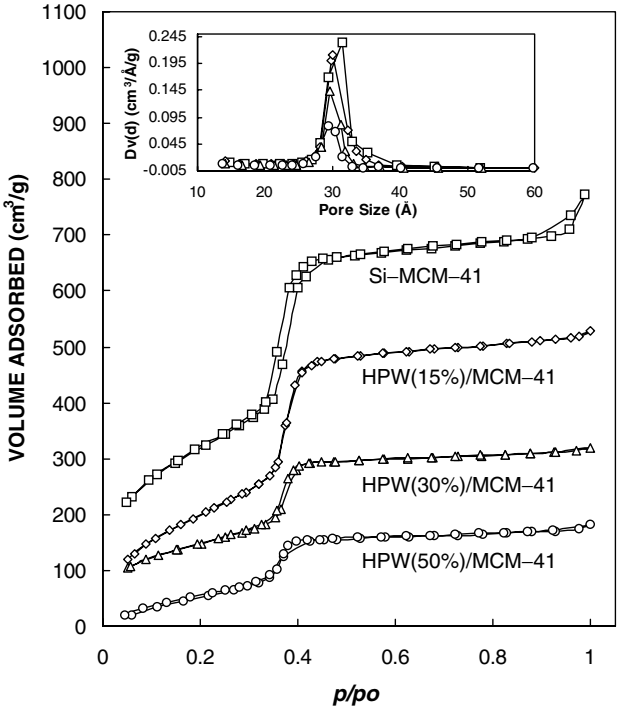

FIG. 2. The effect of HPW loading on the nitrogen adsorption–desorption isotherms and the pore size distribution of HPW/MCM-41 samples.

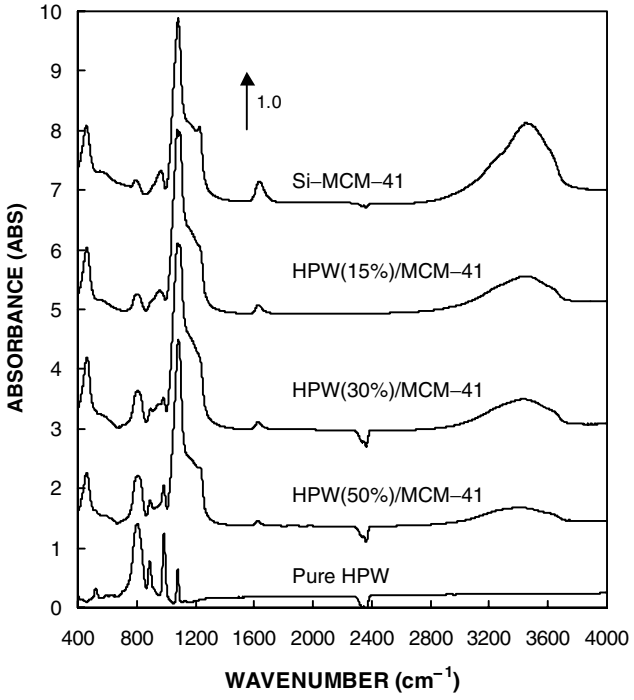

FIG. 3. The effect of HPW loading on the Keggin structures of HPW on HPW/MCM-41 samples.

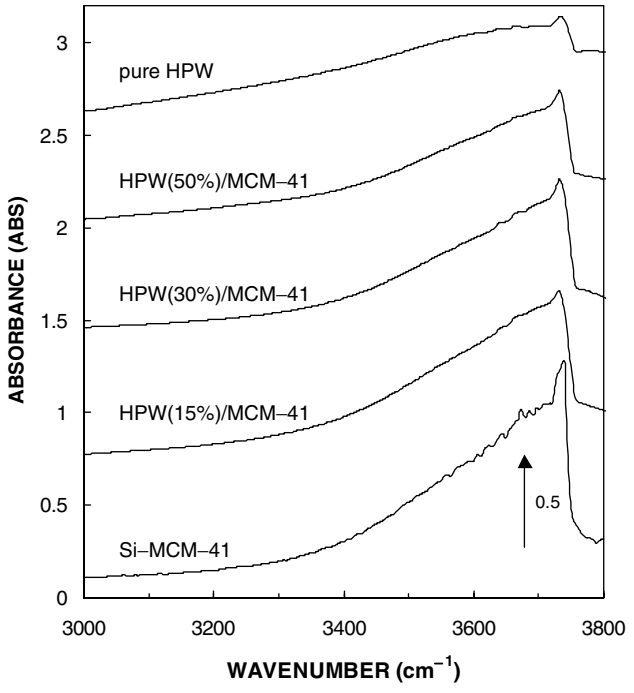

FIG. 4. The effect of HPW loading on the relative coverage of surface hydroxyl groups of HPW/MCM-41 samples.

Surface OH Relative Coverage and Surface Acidity on HPW/MCM-41 Samples

FTIR spectra between 3800 and 3000 cm^{-1} of the Si–MCM-41 and HPW/MCM-41 samples (in Fig. 4) show that the relative coverage of surface hydroxyl groups decreases with increasing HPW loading. In the present work, the Si–MCM-41 sample exhibits many clear absorbance bands, at about 3742, 3729 (shoulder), 3709, 3697, 3687, 3674, 3642, 3622, 3606, and 3574 cm^{-1}. These respective hydroxyls were assigned to isolated silanols and to associated hydroxyls with different degrees of hydrogen bonding (38, 45). The deposition of HPW on Si–MCM-41 results in a clear decrease in the band at 3742 cm^{-1}, assigned to isolated silanols, and in the region 3680–3620 cm^{-1}, associated with bridging OH band. Owing to the rather weak hydroxyl bands of pure HPW, the decreasing absorbance in the aforementioned spectral regions may be due to the coverage of dispersed HPW on the surface of Si–MCM-41 or to the interaction of HPW with surface hydroxyl groups of Si–MCM-41 (Scheme 1). Interaction with these hydroxyls has been reported in the case of impregnation of $Zr(OPr^n)_4$ on siliceous MCM-41 (38). For all the HPW/MCM-41 samples, the absorbance in the 3730-cm^{-1} region, associated with very weakly hydrogen-bonded silanols, was always observed; however, its intensity gradually decreased with increasing amounts of HPW. This suggests that these hydroxyls are not easily available to larger HPW molecules, as is also the case with other larger molecules (38, 45).

The deposition of HPW on Si–MCM-41 is an efficient way to decrease the abundance of surface hydroxyls to a large extent. Table 2 shows a marked decrease in the relative coverage of surface hydroxyls, from 100% for Si–MCM-41 to 29.0% for pure HPW, presumably due to the dispersion and interaction depicted in Scheme 1. Continuous increasing HPW loading further enhances the

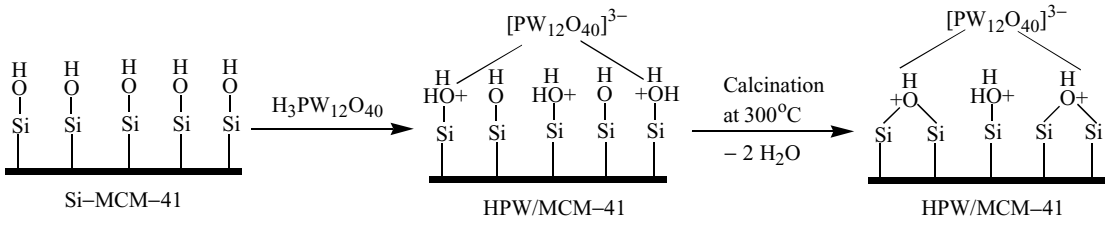

SCHEME 1

TABLE 2

Effect of HPW Loading on Surface OH Relative Coverage and Surface Acidity of HPW/MCM-41 Samples

Sample	–OH relative[a] coverage	B acid[b] (at 1540 cm^{-1})	L acid[b] (at 1445 cm^{-1})	B/L	L/B
Si–MCM-41	100	0	0		
HPW (15%)/MCM-41	70.8	0.38	1.99	0.19	5.24
HPW (30%)/MCM-41	61.1	1.18	2.50	0.47	2.12
HPW (50%)/MCM-41	45.5	4.30	3.39	1.27	0.79
Pure HPW	29.0				

[a] –OH relative coverage is an area fraction percentage (%).
[b] Brønsted and Lewis acidities are quantified into integrated areas of the absorbances at 1540 and at 1445 cm^{-1}, respectively.

abovementioned effects, leading to the stepwise enhancement of hydrophobicity of the HPW/MCM-41 materials. This obviously differs from the observation of Ghanbari-Siahkali *et al.* (37), who showed that with increasing amounts of HPW, the hydrophilicity of the resulting HPW/MCM-41 samples was intensified. The pure HPW and HPW/MCM-41 samples in this work were thermally treated at 300°C for 3 h prior to use; however, those samples were not precalcined in other published studies (26, 36, 37). This preconditioning treatment might remove large numbers of water molecules from these samples and may promote the dispersion of HPW on MCM-41 and the interaction between HPW and Si–OH, further decreasing surface –OH coverage and hydrophilicity.

Figure 5 shows that the surface of Si–MCM-41 does not contain Brønsted or Lewis acidity (38). However, once Si–MCM-41 is loaded with HPW, Brønsted and Lewis acidity are revealed on the HPW/MCM-41 catalysts; acidity increases gradually with increasing HPW loading (from 15 to 50 wt%). In particular, the intensity of the Brønsted acid band increases more rapidly than that of the Lewis acid band. The data in Table 2 show that Brønsted and Lewis acidity, which are, respectively, quantified into integrated areas of the absorbance bands at 1540 and 1445 cm^{-1}, increase stepwise with increasing HPW loading. The HPW loading is <30 wt%, so Lewis acidity dominates; however, as the HPW loading increases to 50 wt%, Brønsted acidity exceeds Lewis acidity. The increase in the Brønsted acid sites from 0.38 to 4.30 is much faster than the increase in the Lewis acid sites, from 1.99 to 3.39 with increasing amounts of HPW from 15 to 50 wt%, resulting in a fast increase in the B/L value from 0.19 to 1.27 and a corresponding reduction in the L/B value from 5.24 to 0.79. The Brønsted and Lewis acids and the B/L value of the HPW/MCM-41 samples can be placed in the following order: Si–MCM-41 $\ll$ HPW (15%)/MCM-41 < HPW (30%)/MCM-41 < HPW (50%)/MCM-41, which is a direct function of the amount of HPW. For the HPW/MCM-41 catalysts, Brønsted acid sites are created due to the presence of small clusters of HPW, a natural protonic acid, while Lewis acid sites might result from the interaction of dispersed HPW with framework SiO_2. The results show that low loading of HPW is beneficial to high dispersion of HPW on Si–MCM-41, inducing more Lewis acid sites than Brønsted acid sites; while a large amount of HPW results in an increasing number of Brønsted acid sites due to the poor dispersion and the formation of small aggregates of HPW on Si–MCM-41. This result further indicates that the categories and the number of the surface acid sites on HPW/MCM-41 catalysts can be adjusted by varying the HPW loading according to the individual reactions.

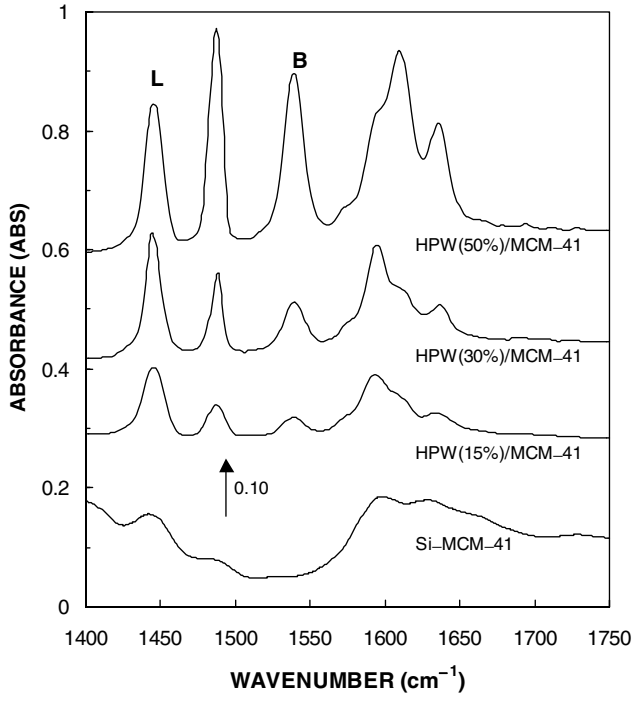

FIG. 5. The effect of HPW loading on the pyridine-adsorption FTIR spectra of HPW/MCM-41 samples.

Catalytic Activity of HPW/MCM-41 Catalysts

For the gas-phase synthesis of MTBE from MeOH and Bu^{t}OH in a continuous fixed-bed reactor, a helium flow of 13 ml min^{-1} must be introduced into the reactor as a carrier gas in order to maintain steady operation and to speed up the adsorption–desorption processes. Figure 6 compares the steady activity and on-stream stability of HPW/MCM-41 catalysts with Si–MCM-41 and commercial Amberlyst-15 catalysts. In this reaction, Si–MCM-41 shows relatively low activity due to the lack of surface acid sites, and the conversion of Bu^{t}OH to MTBE reaches only 18.5 mol%, even at 200°C. The Amberlyst-15 catalyst shows rather high activity, with a selective conversion of about 98.0 mol% Bu^{t}OH to MTBE at temperatures between 80 and 100°C, which favor thermodynamics. Even if the temperature is lowered to 70°C, 72.9 mol% of Bu^{t}OH can still be selectively converted to MTBE. However, the low-temperature activity of HPW/MCM-41 catalysts in this reaction is much lower than that of Amberlyst-15. At 70°C, a low conversion of 22.7 mol% for the former catalyst and 27.3 mol% for the latter catalyst can be realized over the HPW (30%)/MCM-41 and HPW (50%)/MCM-41 catalysts; HPW (15%)/MCM-41 is inactive at that temperature. Obviously, the number of Brønsted acid sites plays a critical role in the low-temperature activity of the catalysts. Owing to the fact that the reaction mechanism involves the formation of isobutyl carbonium ions intermediates and the nucleophilic attack of methanol molecules (11–13), it is assumed that an enhancement of surface acidity will favor the process.

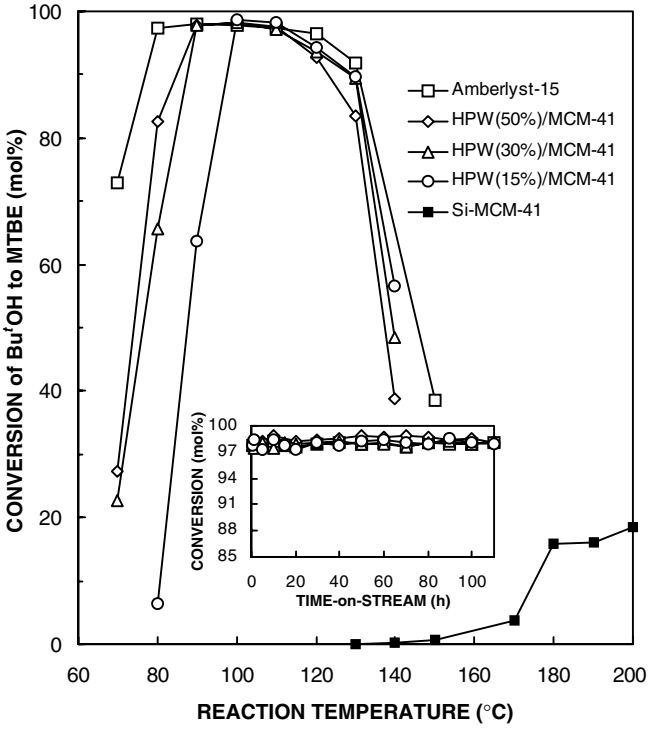

FIG. 6. The comparison of the activity and on-stream stability of Amberlyst-15 and HPW/MCM-41 catalysts for the gas-phase synthesis of MTBE from MeOH and Bu^{t}OH.

TABLE 3

Comparison of Catalytic Activities of Mesoporous Acidic Catalysts with Amberlyst-15 Catalyst[a]

Sample	Conversion (mol%)	Selectivity (%)	Optimal temperature (°C)
H_2SO_4/MCM-41	97.1	99.1	120
NaAlMCM-41	97.9	100	160
HAlMCM-41	98.9	100	130
SO_4^{2-}/ZrO_2/MCM-41	98.6	100	140
HPW (15%)/MCM-41	98.6	100	100
HPW (30%)/MCM-41	98.2	100	90–100
HPW (50%)/MCM-41	98.2	100	90–100
Amberlyst-15	98.0	100	80–100

[a] The gas-phase synthesis of MTBE from MeOH and Bu^{t}OH was carried out in a continuous fixed-bed reactor: 0.20 g of the catalyst, a helium flow of 13 ml/min, a mixture reactant of MeOH and Bu^{t}OH with a molar ratio of 10 : 1, and a WHSV kept at 10 h^{-1}.

However, three HPW/MCM-41 catalysts showed good activity (selective conversion of >98.2 mol% Bu^{t}OH to MTBE) at temperatures close to 100°C, which makes them comparable to that of commercial Amberlyst-15 catalyst. However, the temperature range (in Table 3) within which an ideal conversion can be achieved gradually decreases from 80 to 100°C for Amberlyst-15, to 90–100°C for the HPW (30–50%)/MCM-41 catalysts, and to 100°C for HPW (15%)/MCM-41, which is consistent with the difference of Brønsted acidity. This means that due to the acid-catalyzed characteristics, the apparent activation energy barrier of this reaction can be easily overcome by introducing Brønsted acid sites. This reaction is sensitive to slight changes in temperature; once the temperature exceeds 110°C, the selectivity of by-products such as hydrocarbons and oxygenates will increase, leading to a linear reduction in the selectivity to MTBE with increasing temperature. Based on thermodynamics equilibrium, the higher temperatures will largely promote side reactions over acid catalysts to produce other hydrocarbons or oxygenates. Thus, the bell shape of the selective conversion curves for butanol (in Fig. 6) may be due to the same causes; the descending portions of the curves at higher temperatures correspond to the shift in equilibrium toward a lower yield of MTBE in most exothermic reactions. As shown in Fig. 6, three HPW/MCM-41 catalysts also exhibit high on-stream steady activity, comparable to that of the Amberlyst-15 at 100°C. With increasing time-on-stream up to 110 h, the highly selective conversion of Bu^{t}OH to MTBE remains more or less constant with these catalysts. This might be due to the relatively small diffusion hindrance of these mesoporous catalysts and to their high hydrophobicity.

Comparison of Various Mesoporous Acidic Catalysts; Comparison of Mesostructures

Figure 7 shows that the XRD patterns of uncalcined and calcined NaAlMCM-41 as well as ion-exchanged HAlMCM-41 consist of a strong reflection at around 2.2° (d_{100}) and two weak reflections at 3.7 and 4.3°, implying that these materials have a long-range, ordered mesostructure and well-formed hexagonal pore arrays (31, 46). However, the ion-exchange treatment results in a small loss of crystallinity of the resulting HAlMCM-41. The infrared vibration bands of NaAlMCM-41 (1236, 1084, 966, 799, 574, and 461 cm^{-1}) and HAlMCM-41 (1234, 1090, 964, 799, 568, and 465 cm^{-1}) are very close to the characteristic vibrations of the mesoporous framework of Si–MCM-41 (43, 44). The XRD pattern of the H_2SO_4/MCM-41 material shows that the uniform mesostructure of Si–MCM-41 remains unchanged after the H_2SO_4 adsorption treatment. The structural characterizations of SO_4^{2-}/ZrO_2/MCM-41 also showed that the regular hexagonal structure of Si–MCM-41 with a uniform mesopore size does not change after 41.0 wt% ZrO_2 loading.

The *in situ* FTIR spectrum of H_2SO_4/MCM-41 (Fig. 8), measured after evacuation at 300°C for 5 h, shows an intense absorbance band at around 1409 cm^{-1}, corresponding to the asymmetric stretching frequency of the covalent S=O band (38). After calcination at 600°C for 3 h, the 1409 cm^{-1} band disappears and the same absorbance spectrum as that of Si–MCM-41 in the region 1000–3000 cm^{-1} is restored. It is conceivable in the H_2SO_4/MCM-41 material that H_2SO_4 molecules are merely adsorbed onto the surface of mesopores of Si–MCM-41, that no strong interaction takes place between H_2SO_4 molecules and framework SiO_2, and that the thermal treatment at high temperature in air can, thus, completely remove the adsorbed H_2SO_4 molecules. This band was still observable for SO_4^{2-}/ZrO_2/MCM-41 calcined at 600°C for 3 h but shifted to at about 1363 cm^{-1}. This band is attributed to the covalent S=O band resulting from the chemical interaction between SO_4^{2-} and ZrO_2, often regarded as the characteristic band of SO_4^{2-} of promoted solid acids (47).

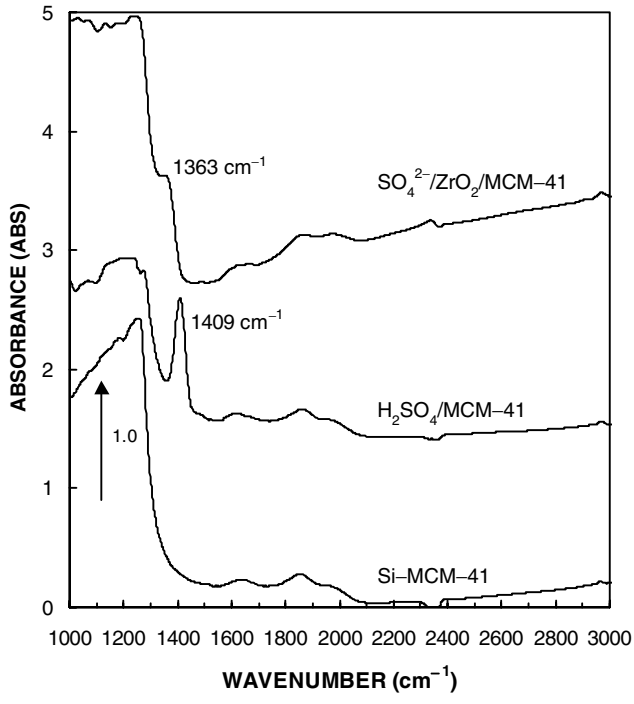

FIG. 8. The S=O vibrational bands of SO_4^{2-}/ZrO_2/MCM-41 and H_2SO_4/MCM-41 samples.

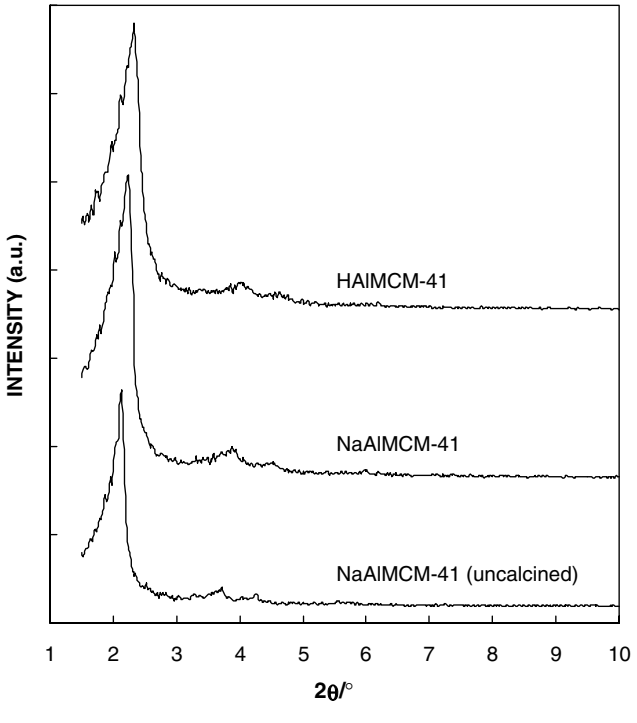

FIG. 7. The effect of the ion-exchange treatment and calcination treatment on the XRD patterns of Al-containing MCM-41 samples.

A sharp inflection is observed on the isotherms of NaAlMCM-41, HAlMCM-41, H_2SO_4/MCM-41, and SO_4^{2-}/ZrO_2/MCM-41 at relative pressures between 0.25 and 0.40, as for Si–MCM-41 and HPW (50%)/MCM-41, showing that these materials have typical mesoporous structures (31, 38, 48–51). However, in addition to the sharp inflection for the above samples, the NaAlMCM-41 and HAlMCM-41 samples show another sharp increase in the adsorbed volume at high relative pressures ($p/po > 0.90$); the other samples showed little or no change in the adsorbed volume in this high relative pressure region. This second inflection, which was attributed to macropore filling or to the filling of interparticle pores (51, 52), may result from the formation of extraframework Al and, thus, from the partial collapse

of the structure induced by the thermal treatment at high temperature.

Table 1 shows that Si–MCM-41, H_2SO_4/MCM-41, NaAlMCM-41, and HAlMCM-41 have a large BET surface of greater than 1000 m^2/g, a pore volume $\geq$1.00 cm^3/g, and a pore diameter >26.7 Å. The ion-exchange treatment and H_2SO_4 adsorption exert a slight negative effect on the BET data of the resulting samples. Compared with NaAlMCM-41, the BET specific surface area, pore volume, and pore diameter of HAlMCM-41 decreased from 1257 to 1122 m^2/g, from 1.01 to 0.99 cm^3/g, and from 28.0 to 26.7 Å, respectively. The BET specific surface area of H_2SO_4/MCM-41 changed slightly; the pore volume and pore diameter showed little change compared to Si–MCM-41. After loading with 41.0 wt% ZrO_2 and 50 wt% HPW, the BET specific surface area, pore volume, and pore diameter of the resulting SO_4^{2-}/ZrO_2/MCM-41 decreased to 688 m^2/g, 0.58 cm^3/g, and 29.3 Å, while the same characteristics of HPW (50%)/MCM-41 decreased to 499 m^2/g, 0.40 cm^3/g, and 29.5 Å. Amberlyst-15 was found to have the extremely low BET surface area of about 50 m^2/g, with an extremely small pore volume of 0.05 cm^3/g; however, the pore volume probably varied during the course of the reaction as a result of the swelling caused by the water formed during the reaction.

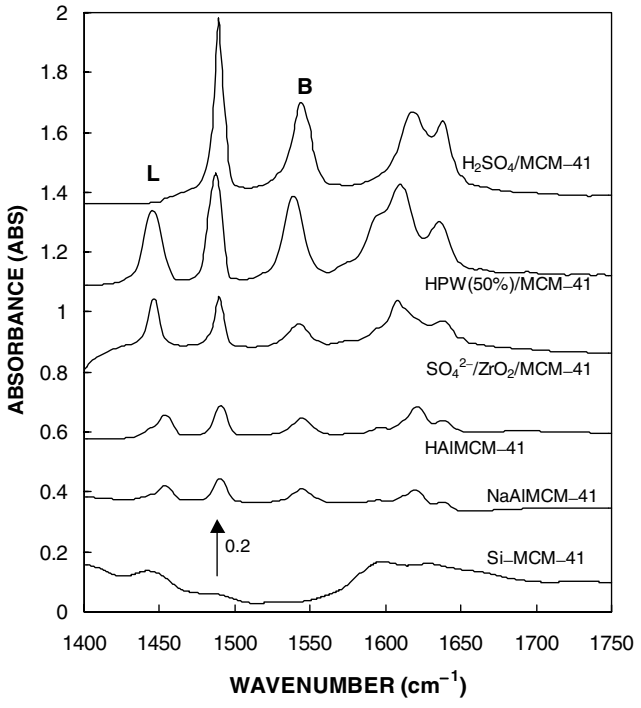

FIG. 9. The pyridine adsorption FTIR spectra of various mesoporous acid catalysts.

Comparison of Surface Acidity and Catalytic Activity

Owing to the incorporation of aluminium and the formation of amorphous silica–alumina at high-temperature calcination, the surface of NaAlMCM-41 contains Brønsted and Lewis acid sites (39, 41, 50, 51). In this study, Brønsted and Lewis acid sites on NaAlMCM-41 were measured to be the integrated areas of 0.68 and 0.59, as shown in Fig. 9 and Table 4. Once ion exchanged into HAlMCM-41, the surface Brønsted and Lewis acid sites increased further, to 0.88 and 0.95, respectively. The leaching of framework aluminum during the ion-exchange of NaAlMCM-41 is detectable by ICP analysis, and the Si : Al ratio of HAlMCM-41 increases from the initial 22 to 25. The enhancement of surface acidity of HAlMCM-41 is due to the removal and replacement of balance Na^+ cations with negatively charged framework aluminium atoms by H^+ protons. However, the increase in the number of Lewis acid sites was greater than that of the Brønsted acid sites, resulting in a decrease in the B/L value from 1.15 to 0.93. For SO_4^{2-}/ZrO_2/MCM-41, the Brønsted and Lewis acid sites increased to 1.21 and 1.43, respectively, with a B/L value of 0.85. The respective Brønsted and Lewis acid sites of HPW (50%)/MCM-41 increased to an even greater extent, to 4.30 and 3.39, with a B/L value of 1.27. It is interesting that only Brønsted acid centers are present in H_2SO_4/MCM-41, with a value of 4.32. This can be explained by the fact that, H_2SO_4 acid being an inorganic acid, adsorption of H_2SO_4 molecules only introduces protonic centers on the surface of Si–MCM-41. The relative concentrations of the total acid sites in all the mesoporous materials listed in Table 4 can be placed in the following decreasing order: HPW (50%)/MCM-41 > H_2SO_4/MCM-41 > SO_4^{2-}/ZrO_2/MCM-41 > HAlMCM-41 > NaAlMCM-41 $\gg$ Si–MCM-41.

TABLE 4

Pyridine Adsorption Data on Various Mesoporous Samples

Sample	B acid[a] (at 1540 cm^{-1})	L acid[a] (at 1445 cm^{-1})	B/L
Si–MCM-41	0	0	
H_2SO_4/MCM-41	4.32	0	
NaAlMCM-41	0.68	0.59	1.15
HAlMCM-41	0.88	0.95	0.93
SO_4^{2-}/ZrO_2/MCM-41	1.21	1.43	0.85
HPW (50%)/MCM-41	4.30	3.39	1.27

[a] Brønsted and Lewis acidities are quantified into integrated areas of the absorbances at 1540 and at 1445 cm^{-1}, respectively.

Figure 10 illustrates that the difference in the surface acidity on various mesoporous catalysts also strongly affects their activity for the gas-phase synthesis of MTBE. For all the catalysts, with the exception of Si–MCM-41, the relationship between the selective conversion and the reaction temperatures varied in the same way, to give a bell-shaped curve. For each catalyst, there is an optimal temperature range at which the highest conversion can be obtained (Table 3). The optimal reaction

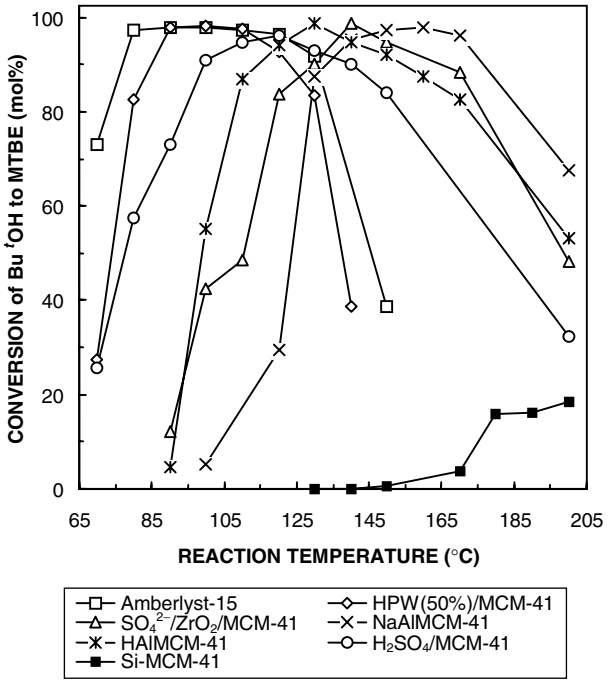

FIG. 10. The relationship between the activity of various acid catalysts for the gas-phase synthesis of MTBE and the reaction temperature.

temperatures shifts gradually to higher values in the following order: Amberlyst-15 (80–100°C) < HPW (50%)/MCM-41 (90–100°C) < H_2SO_4/MCM-41 (120°C) < HAlMCM-41 (130°C) < SO_4^{2-}/ZrO_2/MCM-41 (140°C) < NaAlMCM-41 (160°C) ≪ Si–MCM-41 (>200°C). This is approximately consistent with the decreasing acidities. The exception of SO_4^{2-}/ZrO_2/MCM-41 may be due to the complexity of the sulfated-ZrO_2 superacid system.

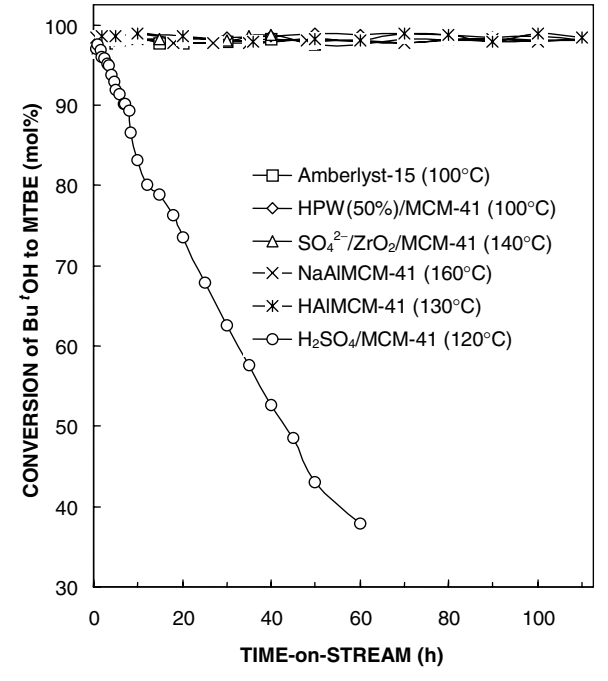

FIG. 11. The comparison of the stability of on-stream Amberlyst-15 and various mesoporous acid catalysts for the gas-phase synthesis of MTBE.

Over the NaAlMCM-41 catalyst, only 29.3 mol% selective conversion of Bu^{t}OH to MTBE was obtained at 120°C; however, at this temperature, the conversion on HAlMCM-41 increases to 94.0 mol%, which can be ascribed to an improvement of surface acidity on HAlMCM-41 following the ion-exchange treatment. The NaAlMCM-41 catalyst shows higher activity and fewer side reactions at high temperatures than does HAlMCM-41. For all the catalysts except Si–MCM-41, a high temperature results in strong side reactions, catalyzing the formation of other oxygenates and hydrocarbons and leading to a fast decrease in the MTBE yield. The bell-shape curve for the selective conversion of butanol in Fig. 10 may have the same cause as that of HPW/MCM-41. As expected, H_2SO_4/MCM-41 exhibits higher activity at low temperature than the NaAlMCM-41, HAlMCM-41, and SO_4^{2-}/ZrO_2/MCM-41 catalysts, due to the fact that H_2SO_4 is a strong protonic acid. Even at 70°C, about 25.6 mol% conversion is reached, which is less than over HPW (50%)/MCM-41 and Amberlyst-15 catalysts.

Figure 11 illustrates the on-stream activity of various mesoporous catalysts, in which the reactions are carried out at the respective optimal reaction temperatures. With an increase in time-on-stream to 110 h and with the exception of H_2SO_4/MCM-41, the highly selective conversion of Bu^{t}OH to MTBE hardly changes, showing the excellent stability of these catalysts. This is attributed to the relatively small diffusion hindrance over mesoporous catalysts, in which the adsorption–desorption processes readily occur, decelerating the deactivation of the catalysts by coking. As expected, the catalytic activity of the H_2SO_4/MCM-41 catalyst displays an almost a linear reduction of the conversion to 37.8 mol% for 60 h at 120°C. This was ascribed to the leaching of mobile H_2SO_4 molecules on Si–MCM-41 in the gas–liquid stream. The aforementioned comparison further illustrates the potential advantages of mesoporous materials as acidic catalysts for the gas-phase synthesis of MTBE or other acid-catalyzed reactions.

CONCLUSIONS

The results show that HPW loading has a notable effect on the intensity of the main XRD reflection [100] peak of the Si–MCM-41 support, and the height of this peak has an effect inverse to the extent of HPW loading. The regular mesostructure of Si–MCM-41 with a uniform mesopore size is constant after a 50-wt% HPW loading. When the loading of HPW is lower than 15 wt%, it is difficult to detect the Keggin structure of HPW on HPW/MCM-41; however,

when the amount of HPW is greater than 30 wt%, the Keggin structure IR bands of HPW on HPW/MCM-41 gradually intensify with increasing HPW loading. The surface acidity and hydrophobicity of the HPW/MCM-41 catalysts increase stepwise with an increase in the HPW loading. The ratio of Brønsted acidity to Lewis acidity on HPW/MCM-41 can be adjusted by varying the amounts of HPW. An HPW-supported mesoporous catalyst (HPW/MCM-41) showed excellent catalytic activity and on-stream stability for the gas-phase synthesis of MTBE at quite low temperatures, <100°C.

There is only Brønsted acidity on H_2SO_4/MCM-41, resulting from the adsorbed protonic H_2SO_4 molecules. The total number of acid sites on the mesoporous acid catalysts can be placed in the following order: HPW (50%)/MCM-41 > H_2SO_4/MCM-41 > SO_4^{2-}/ZrO_2/MCM-41 > HAlMCM-41 > NaAlMCM-41 ≫ Si–MCM-41. The catalytic activity of various acid catalysts increased in the following order: Amberlyst-15 ≈ HPW (50%)/MCM-41 > H_2SO_4/MCM-41 > HAlMCM-41 > SO_4^{2-}/ZrO_2/ MCM-41 > NaAlMCM-41 ≫ Si–MCM-41. The optimal reaction temperature for achieving the highest conversion gradually shifts to higher temperatures: Amberlyst-15 (80–100°C) < HPW (50%)/MCM-41 (90–100°C) < H_2SO_4/MCM-41 (120°C) < HAlMCM-41 (130°C) < SO_4^{2-}/ZrO_2/MCM-41 (140°C) < NaAlMCM-41 (160°C) ≪ Si–MCM-41 (>200°C), approximately in agreement with the sequence of decreasing surface acidity. The exception of SO_4^{2-}/ZrO_2/MCM-41 in this arrangement could be related to the complexity of the sulfated-ZrO_2 superacid. All the mesoporous acid catalysts, except for H_2SO_4/MCM-41, exhibit high on-stream stability at respective optimal reaction temperatures for this reaction. The rapid deactivation of the H_2SO_4/MCM-41 catalyst may be due to the leaching of mobile H_2SO_4 molecules on Si–MCM-41 in the reaction stream.

REFERENCES

1. Collignon, F., Mariani, M., Moreno, S., Remy, M., and Poncelet, G., *J. Catal.* **166**, 53 (1997).
2. Nikolopoulos, A. A., Kogelbauer, A., Goodwin, J. G., Jr., and Marcelin, G., *Catal. Lett.* **39**, 173 (1996).
3. Peaff, G., *Chem. Eng. News* **101**, 8 (1994).
4. Gregerson, L. N., Siegel, J. S., and Baldridge, K. K., *J. Phys. Chem. A* **104**, 106 (2000).
5. Keller, A. A., Sandall, O. C., Rinker, R. G., Mitani, M. M., Bierwagen, B., and Snodgrass, M. J., *Ground Water Monit. Remediation* **20**, 114 (2000).
6. Kharoune, M., Pauss, A., and Lebeault, J. M., *Water Res.* **35**, 1665 (2001).
7. Amberg, A., Rosner, E., and Dekant, W., *Toxicol. Sci.* **61**, 62 (2001).
8. Erdal, S., and Goldstein, B. D., *Annu. Rev. Energy Environ.* **25**, 765 (2000).
9. Nadim, F., Zack, P., Hoag, G. E., and Liu, S. L., *Energy Policy* **29**, 1 (2001).
10. Horvath, T., Seiler, M., and Hunger, M., *Appl. Catal. A* **193**, 227 (2000).
11. Nicolaides, C. P., Stotijn, C. J., van der Veen, E. R. A., and Visser, M. S., *Appl. Catal.* **103**, 223 (1993).
12. Hutchings, G. J., Nicolaides, C. P., and Scurrell, M. S., *Catal. Today* **15**, 23 (1992).
13. Le Van, Mao, R., Le, T. S., Faibairn, M., Muntasar, A., Xiao, S., and Denes, S., *Appl. Catal. A* **185**, 221 (1999).
14. Kim, J. S., Kim, J. M., Seo, G., Park, N. C., and Niiyama, S., *Appl. Catal.* **37**, 45 (1988).
15. Adams, J. M., Martin, K., McCabe, R. W., and Murray, S., *Clays Clay Miner.* **34**, 597 (1986).
16. Quiroga, M. E., Figoli, N. S., and Sedran, U. A., *J. Chem. Eng.* **67**, 199 (1997).
17. Chu, P., and Kühl, G. H., *Ind. Eng. Chem. Res.* **26**, 365 (1987).
18. Nikolopoulos, A. A., Oukaci, R., Goodwin, J. G., Jr., and Marcelin, G., *Catal. Lett.* **27**, 149 (1994).
19. Le Van, Mao, R., Carli, R., Ahlafi, H., and Ragaini, V., *Catal. Lett.* **6**, 321 (1990).
20. Collignon, F., Leonders, R., Martens, J. A., Jacobs, P. A., and Poncelet, G., *J. Catal.* **182**, 302 (1999).
21. Misono, M., *Catal. Rev.–Sci. Eng.* **29**, 269 (1987); **30**, 339 (1988).
22. Kozhevnikov, I. V., *Catal. Rev.–Sci. Eng.* **37**, 311 (1995).
23. Okuhara, T., Mizuno, N., and Misono, M., *Adv. Catal.* **41**, 113 (1996).
24. Corma, A., *Chem. Rev.* **95**, 559 (1995).
25. Misono, M., Mizuno, N., Katamura, K., Kasei, A., Konishi, Y., Sakata, K., Okuhara, T., and Yoneda, Y., *Bull. Chem. Soc. Jpn.* **55**, 400 (1982).
26. Blasco, T., Corma, A., Martinez, A., and Martinez-Escolano, P., *J. Catal.* **177**, 306 (1998).
27. Nowinska, K., Fiedorow, R., and Adamiec, J., *J. Chem. Soc. Faraday Trans.* **87**, 749 (1991).
28. Cheng, W.-C., and Luthra, N. P., *J. Catal.* **109**, 163 (1988).
29. Rao, K. M., Gobetto, R., Lannibello, R., and Zecchina, A., *J. Catal.* **119**, 512 (1989).
30. Mastikhin, V. M., Terkikh, W., Timofeeva, M. N., and Krivoruchko, O. P., *J. Mol. Catal. A* **95**, 135 (1995).
31. Krege, C. T., Leonowicz, M. E., Roth, W. J., Vartuli, J. C., and Beck, J. S., *Nature* **359**, 710 (1992).
32. Kosslick, H., Lischike, G., Parlitz, B., Storek, W., and Fricke, R., *Appl. Catal. A* **184**, 49 (1999).
33. Corma, A., Martinez, A., Martinez-Soria, V., and Monton, J. B., *J. Catal.* **153**, 25 (1995).
34. Corma, A., Martinez, A., and Martinez-Soria, V., *J. Catal.* **169**, 480 (1997).
35. Xia, Q.-H., Hidajat, K., and Kawi, S., *Catal. Today* **68**, 255 (2001).
36. Kozhevnikov, I. V., Sinnema, A., Jansen, R. J. J., Pamin, K., and van Bekkum, H., *Catal. Lett.* **30**, 241 (1995).
37. Ghanbari-Siahkali, A., Philippou, A., Dwyer, J., and Anderson, M. W., *Appl. Catal. A* **192**, 57 (2000).
38. Xia, Q.-H., Hidajat, K., and Kawi, S., *Chem. Commun.* 2229 (2000); *J. Catal.* **205**, 318 (2002).
39. Corma, A., Fornes, V., Navarro, M. T., and Perez-Pariente, J., *J. Catal.* **148**, 569 (1994).
40. Sayari, A., *Chem. Mater.* **8**, 1480 (1996).
41. Mokaya, R., and Jones, W., *Chem. Commun*. 983 (1996).
42. Corma, A., Grange, M. S., Gonzales-Alfaro, V., and Orchilles, A. V., *J. Catal.* **159**, 375 (1996).
43. Xia, Q.-H., Hidajat, K., and Kawi, S., *Mater. Lett.* **42**, 102 (2000); *Chem. Lett.* 654 (2001).
44. Xia, Q.-H., Hidajat, K., and Kawi, S., *Stud. Surf. Sci. Catal.* **129**, 49 (2000); **135**, 205 (2001).

45. Jentys, A., Pham, N. H., and Vinek, H., *J. Chem. Soc. Faraday Trans.* **92**, 3287 (1996).
46. Chen, C.-Y., Li, H.-X., and Davis, M. E., *Microporous Mater.* **10**, 283 (1997).
47. Drago, R. S., and Kob, N., *J. Phys. Chem. B* **101**, 3360 (1997).
48. Mokaya, R., Jones, W., Luan, Z., Alba, M. D., and Klinowski, J., *Catal. Lett.* **37**, 113 (1996).
49. Branton, P. J., Hall, P. G., and Sing, K. S. W., *Chem. Commun.* 1257 (1993).
50. Luan, Z., Cheng, C.-F., He, H., and Klinowski, J., *J. Phys. Chem.* **99**, 10590 (1995).
51. Luan, Z., He, H., Zhou, W., Cheng, C.-F., and Klinowski, J., *J. Chem. Soc. Faraday Trans.* **91**, 2955 (1995).
52. Chakraborty, B., and Viswanathan, B., *Catal. Today* **49**, 253 (1999).